Nanotechnology Perceptions
ISSN 1660-6795
www.nano-*ntp.com*

AC Conductivity And Time–Temperature Superposition Scaling In Reduced Graphene Oxide–Zinc Selenide Composite

Abdulla Bin Rahaman*

Department of Physics, Uluberia College, Uluberia, 711315, India.
**Corresponding author: abdullabinrhmn@gmail.com*

In this study, a comprehensive analysis of the AC conduction mechanism in a reduced graphene oxide–zinc selenide (RGO–ZnSe) composite is presented across a wide temperature range from 90K to 473K. The conductivity isotherms show a frequency-independent conductivity at lower frequencies, transitioning to dispersive conductivity at higher frequencies, which follows a power-law relationship. The temperature-invariant frequency exponent 's' suggests that charge carriers undergo phonon-assisted quantum mechanical tunneling between defect states within the studied sample. Impedance spectroscopy reveals a single semi-circular arc at all temperatures, indicating a Debye-like relaxation process with a consistent relaxation time throughout the entire temperature range. Furthermore, the sample adheres to the time-temperature superposition principle, as demonstrated by the universal scaling of its conductivity isotherms. These findings provide valuable insight into the transport mechanisms of the RGO-based composite system and offer a foundation for exploring transport behavior in other disordered materials.

Keywords: graphene composite, ac conductivity, conductivity scaling, quantum tunnelling.

1. Introduction: In recent years, graphene oxide (GO) nanostructures have garnered significant research attention due to their ability to offer an efficient, reliable, and cost-effective method for the scalable production of graphene sheets in solution [1-3]. When fully oxidized, graphene oxide exhibits insulating properties with a band gap of approximately 4 eV, which can be adjusted to several tenths of an electronvolt in its reduced state, commonly referred to as reduced graphene oxide (RGO) [4]. RGO stands out as a promising material for applications in biosensors, nanoelectronics, photocatalysts, supercapacitors, and transistors due to its ease of processing, lightweight nature, mechanical flexibility, and ability to cover large areas. Its extensive surface area, coupled with a variety of oxygen functional groups also makes it an ideal template for the fabrication of nanophase composite materials [5-8].

Among various semiconductor materials, zinc-based nanostructures have gained significant attention for their potential applications in optoelectronics [9]. Zinc selenide (ZnSe), with a band gap of 2.67 eV, is regarded as an ideal material for photodetectors, blue laser diodes, light-emitting diodes, sensors, and photocatalytic applications [10, 11]. One of the major drawbacks of ZnSe in optoelectronic applications is its low electrical conductivity and carrier

mobility. Recent research has suggested that creating composites with materials like carbon nanotubes or reduced graphene oxide could help address this issue. [12]

The optoelectronic characteristics of RGO composites are closely linked to the conductivity and mobility of the samples. Reduced graphene oxide sheets are known to exhibit a significant level of disorder, with charge transport properties influenced by the ratio of sp^2 to sp^3 domains. Gaining a deeper understanding of the electron transport mechanism in two-dimensional layered RGO sheets is essential, as the conduction mechanism is crucial for the performance of various optoelectronic applications based on such materials. Several studies have explored the transport phenomena in RGO and RGO-based composites. Daeha et. al. modeled RGO as a collection of isolated sp^2 graphene domains surrounded by sp^3 functionalized oxidized regions [13]. In electronic transport, electrons tunnel between graphene domains via the oxidized areas. At low temperatures, the transport in RGO is primarily governed by Coulomb blockade and variable-range hopping (VRH) conduction, which is also influenced by the sp^2 fraction within the RGO matrix. The Efros−Shklovskii VRH mechanism in highly soluble zinc tetra-tert-butyl phthalo cyanine−reduced graphene oxide blend samples have been reported [14]. DC conductivity provides macroscopic values as it reflects charge transfer across the sample, influenced by the potential barriers at the ends. In contrast, frequency-dependent conductivity measures the oscillatory movement of charges. A. Sarkar et al. investigated electrical measurements on zinc telluride dispersed RGO matrix, observing a three dimensional-VRH transport process for DC conduction across 85K-280K temperature range. Nonetheless, frequency-dependent conductivity was dominated by phonon-assisted quantum-mechanical tunneling (QMT) between defect states [15]. Similarly, for the RGO-ZnS composite, QMT of electrons between defect states was observed [16]. Therefore, examining both DC and AC conductivity in RGO-based composites provides valuable insights into the underlying charge transport mechanisms.

In our previous study, temperature-dependent (84K–473K) DC electrical properties of the RGO-ZnSe composite have been investigated to explore the potential charge transport mechanisms. The Resistance Curve Derivative Analysis method indicated a conduction mechanism consistent with Mott's three-dimensional variable-range hopping at lower temperatures (84 K–280 K). At higher temperatures (290 K–473 K), an Arrhenius-like transport behavior was observed [12]. This work primarily focuses on the temperature-dependent (90 K–473 K) AC conductivity and conductivity relaxation processes of the RGO-ZnSe composite, which reveal quantum mechanical tunneling (QMT) between localized states throughout the entire temperature range. The structural and morphological properties were characterized using X-ray diffraction (XRD), high-resolution transmission electron microscopy (HRTEM), and scanning electron microscopy (SEM). This study provides valuable insights into the electrical conduction mechanisms in RGO-based composite materials.

2. Experimental Details:

Materials Synthesis and Characterization: Graphene oxide was synthesized from graphite powder using a modified Hummers method [17]. To prepare the RGO-ZnSe composite, 40 mg

of GO was dispersed in a mixture of ethylene glycol ($C_2H_6O_2$; EG) and ethylenediamine ($C_2H_8N_2$; ED) at a 24:1 volume ratio, followed by ultrasonic treatment for 1 hour. 0.5 mmol zinc acetate dihydrate, 0.5 mmol sodium selenite, and 0.4 g of poly(vinylpyrrolidone) (PVP) were added to the GO suspension and stirred for 30 minutes. The mixture was then transferred to a Teflon-lined stainless-steel autoclave and heated in an oven at 180°C for 12 hours. Afterward, the product was centrifuged and washed multiple times with distilled water and ethanol. The washed samples were dried under vacuum at room temperature for 6 hours, and the final product was designated as RGO-ZnSe.

The crystalline structures of the samples were analyzed using X-ray diffraction (XRD, Rigaku-Miniflex II) with Cu K_α radiation (λ = 1.5418 Å), operated at 30 kV and 10 mA. Surface morphology was examined using a field emission scanning electron microscope (Zeiss, operating at 5 keV) and a transmission electron microscope (JEOL-JEM 2100F, operating at 200 keV). For temperature-dependent measurements, the samples were placed in a liquid nitrogen-cooled dipstick cryostat, maintained at a vacuum pressure of 5×10^{-6} mbar during data collection. Temperature control was achieved using a custom-built controller, providing stability of ± 0.5 K across the entire temperature range. The frequency-dependent conductivity (100Hz–1MHz) of the RGO-ZnSe composite was measured using an Agilent 4294A impedance analyzer.

Sample Fabrication: The RGO-ZnSe powder was dispersed in deionized water at a concentration of 20 mg/mL and sonicated for 10 minutes. The samples were fabricated in an indium tin oxide (ITO)/active layer/Al structure using the following procedure. The RGO-ZnSe solution was spin-coated onto patterned ITO substrates at 1000 rpm for 30 seconds and then dried under vacuum at 80°C for 15 minutes. Finally, an aluminium (Al) electrode was deposited on top by thermal evaporation.

3. Results and Discussions: The XRD patterns of ZnSe and RGO-ZnSe composite (Figure 1) reveal diffraction peaks that correspond to the cubic zinc blende structure, consistent with the standard XRD data (JCPDS card no. 37163, a = 5.668 Å). For ZnSe, prominent diffraction peaks are observed at ~27.2°, 45.2°, and 53.5°, which are attributed to the (111), (220), and (311) planes, respectively [18]. The XRD pattern of the RGO-ZnSe composite closely resembles that of ZnSe, suggesting that the incorporation of RGO does not impact the crystallinity or phase structure of ZnSe. The individual ZnSe nanoparticles within the microspheres are estimated to have a size of approximately 8 nm, as determined using the Debye−Scherrer equation.

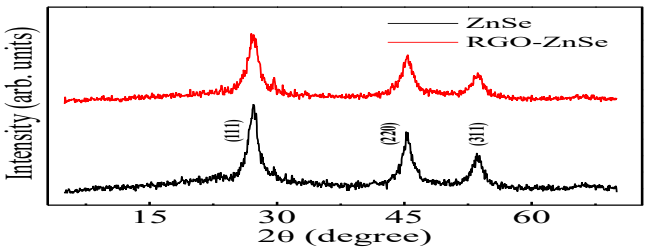

Figure 1: XRD patterns of ZnSe and RGO-ZnSe composite

The microstructures of the synthesized RGO-ZnSe composite were analyzed using SEM and TEM images, shown in Figure 2(a) and 2(b), respectively. As depicted in Figure 2, the large 2D RGO mats are intertwined with ZnSe particles. After subjecting the RGO-ZnSe composites to strong ultrasonication for dispersion, the TEM image demonstrates the strong coupling of ZnSe particles to the RGO sheets.

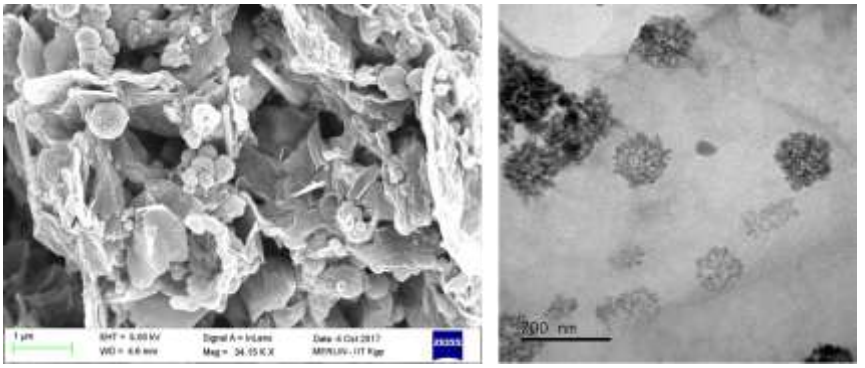

Figure 2: (a) SEM and (b) TEM images of RGO-ZnSe composite.

To investigate the frequency-dependent charge transport and relaxation behavior in the RGO-ZnSe composite, impedance spectroscopy measurements were conducted on an RGO-ZnSe thin film with a top-bottom electrode configuration (Figure 3(a)) across a temperature range of 90 K to 473 K. Figure 3(b) presents the Cole-Cole plot at different temperatures, which shows the imaginary impedance (Z″) as a function of the real impedance (Z′). In this plot, points near the origin represent the high-frequency region, while the low-frequency region is accessed by moving to the right from the origin. A single semi-circular arc is observed at all temperatures, indicating a Debye-like relaxation process governed by a single relaxation time across the entire temperature range [19]. The impedance data were fitted using a single R-CPE (constant phase element) equivalent circuit as shown in the inset of Figure 3(c). Such an equivalent model is employed to determine parameters such as series resistance (R_s), transport resistance, and recombination resistance. The series resistance is associated with the contact layers, electrodes, and connecting leads. The constant phase element is used to model the inhomogeneous nature of the active layer, which features a distribution of recombination times for the charge carriers [20]. From Figure 3(b), it is evident that with an increase in temperature, the diameter of the semicircle decreases. This is in line with the decrease in resistance values (R) with an increase in temperature obtained from fitting parameters. The fitting parameters are tabulated in Table 1. The relaxation time ($\tau = RC$) of charge carriers was calculated from the fitting parameters, and it remains nearly constant (~2 ms), as shown in Figure 3(c).

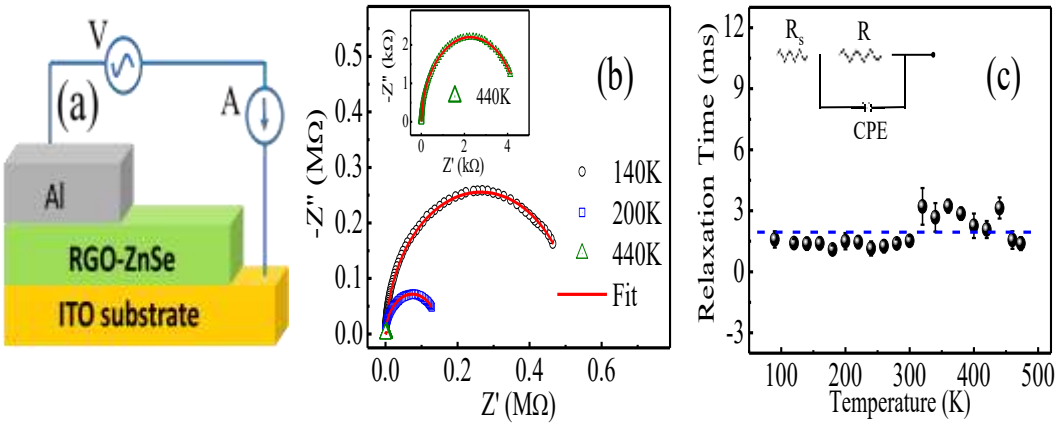

Figure 3: (a) The schematic diagram illustrates the sample configuration used for impedance measurements. (b) The Cole-Cole plot of RGO-ZnSe is presented at various temperatures, with the data at 440K appearing as a single point on the plot. The inset displays the Cole-Cole plot at 440K on an expanded scale. The experimental data are represented by scattered points, while the solid red lines correspond to the fitting results. (c) The charge carrier relaxation time at different temperatures is shown with error bars, which represent the variation observed in measurements conducted on identical samples. The error bars are minimal and are not clearly visible for some data points. The inset displays the equivalent circuit used to fit the impedance data.

Table 1: Cole-Cole plot fitting parameters of RGO-ZnSe composite at different temperatures:

Temp (K)	R_S (Ω)	R (kΩ)	CPE-T (Q)	CPE-P (n)	C (Farad)
90	1420	850.38	2.13×10^{-9}	0.98	1.87×10^{-9}
120	1319	747.81	2.29×10^{-9}	0.97	1.88×10^{-9}
140	1024	529.37	2.97×10^{-9}	0.98	2.61×10^{-9}
160	640	310.93	4.81×10^{-9}	0.99	4.50×10^{-9}
180	472	219.88	6.54×10^{-9}	0.96	4.98×10^{-9}
200	270	148.11	1.16×10^{-8}	0.98	1.02×10^{-8}
220	227	120.95	1.37×10^{-8}	0.98	1.20×10^{-8}
240	166	80.02	1.88×10^{-8}	0.96	1.44×10^{-8}
260	120	58.56	2.62×10^{-8}	0.97	2.15×10^{-8}
280	94	46.94	3.38×10^{-8}	0.98	2.97×10^{-8}
300	61	33.93	5.44×10^{-8}	0.97	4.48×10^{-8}
320	28	34.24	1.21×10^{-7}	0.98	1.08×10^{-7}
340	22	25.31	1.57×10^{-7}	0.98	1.40×10^{-7}
360	16	18.20	2.11×10^{-7}	0.97	1.77×10^{-7}
380	12	11.89	2.70×10^{-7}	0.98	2.40×10^{-7}

400	12	8.21	3.12×10^{-7}	0.98	2.76×10^{-7}
420	8	5.54	4.52×10^{-7}	0.97	3.76×10^{-7}
440	4	4.55	7.74×10^{-7}	0.98	6.90×10^{-7}
460	7	3.46	4.82×10^{-7}	0.99	4.52×10^{-7}
473	5	2.09	7.09×10^{-7}	0.99	6.63×10^{-7}

From the impedance data, the frequency-dependent AC conductivity (σ_{ac}) at various temperatures is extracted, as shown in Figure 4(a). Several observations can be made from this plot: i) $\sigma(\omega)$ remains constant up to a characteristic frequency ω_c; ii) ω_c decreases with decreasing temperature; and iii) for $\omega > \omega_c$, $\sigma(\omega)$ varies with ω^s due to the formation of small capacitors involving RGO sheets in the RGO-ZnSe composite. The frequency-dependent conductivity of the large-area RGO-ZnSe composite can be explained using the universal empirical relation, as represented by the corresponding equation [21-24]

$$\sigma(\omega) = \sigma_{dc} + A\omega^s \qquad (1)$$

Where σ_{dc} represents the DC conductivity, A is a constant that shows slight temperature dependence, and the frequency exponent s is less than or equal to unity. It is worth noting that AC conductivity in various disordered solids and 2D-MoS_2 systems has been extensively studied using this formalism. Almond and West further modified the expression to incorporate the crossover frequency (ω_c). In their formulation, the equation for conductivity was modified to include this frequency and it became [25-26]

$$\sigma(\omega) = \sigma_{dc}\left[1 + \frac{\omega}{\omega_c}\right]^s \qquad (2)$$

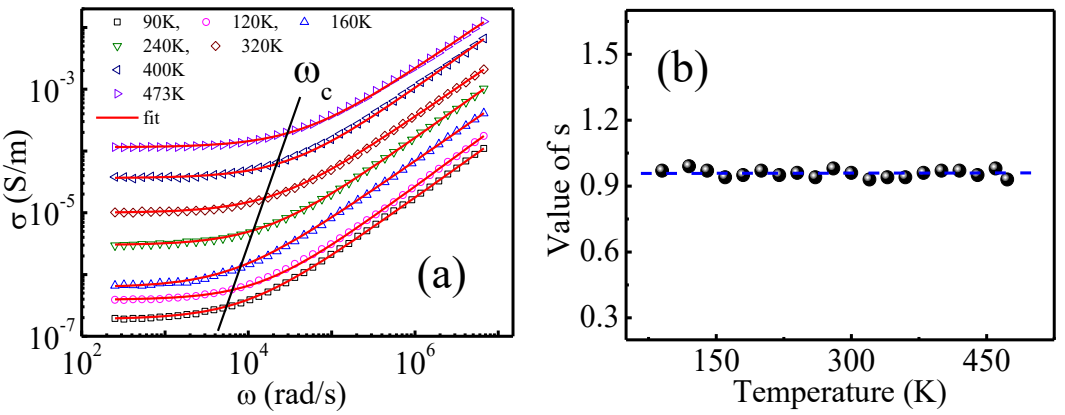

Figure 4: (a) AC conductivity curves at different temperatures, the solid lines are the best fits to equation (1). ω_c is the onset frequency above which conductivity becomes frequency-dependent. (b) Variation of frequency exponent s with temperature. The solid line is a guide to eye.

The data collected for the RGO-ZnSe composite were fitted to the aforementioned equation. From these fits, the values for σ_{dc}, ω_c, and s were determined. The temperature dependence of the frequency exponent s, as obtained from the conductivity spectra fits, is shown in Figure 4(b). It was found that the value of s is approximately 0.95 and exhibited only a weak temperature dependence over the measured temperature range (90 K–473 K). Based on this, it can be concluded that the ac conductivity mechanism is driven by phonon-assisted tunnelling between defect states, a process referred to in the literature as Quantum Mechanical Tunnelling in disordered solids.

Furthermore, it is worth noting from Figure 4(a) that the crossover frequency values increase with DC conductivity, as suggested by Barton-Nakajima-Namikawa [24]. This validated that the conductivity arises from the diffusion of charge carriers across the network. A further analysis can be made by scaling the conductivity spectra based on the characteristics of the curves shown in Figure 5. Additionally, the Almond-West formalism predicts the time-temperature superposition principle, which suggests that the conductivity relaxation process is independent of both time and temperature. With this principle in mind, the conductivity axis scaled using σ_{dc} and the frequency axis using ω_c (the crossover frequency). The figure reveals that the normalized conductivity, plotted against the reduced frequency at various temperatures, merges into a single master curve. This overlapping of conductivity isotherms into one curve indicates a single relaxation process that is independent of both temperature and time in the RGO-ZnSe system under an AC field. A similar time-temperature independent relaxation process has also been observed in CVD-grown MoS_2, polymers, and other RGO-based nanocomposites [16,24,27,28].

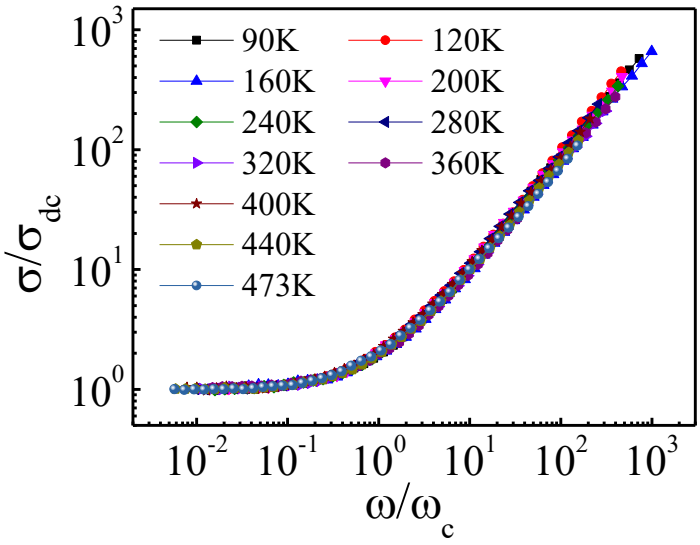

Figure 5: AC conductivity scaling at different temperatures.

DC and AC conductivities in disordered semiconductors arise from different charge transport mechanisms. For DC conductivity, the transport mechanism depends on factors like the band

gap, available thermal energy, and the distribution of localized states. In case of RGO-ZnSe composite, at low temperatures, when thermal energy is insufficient to overcome the band gap, charge carriers follow the Mott 3D variable range hopping process. However, when thermal energy is adequate, DC conductivity occurs via direct band-to-band conduction. In contrast, AC conductivity results from relaxation processes such as correlated barrier hopping, quantum mechanical tunneling, small polaron, and large polaron tunneling. During AC conduction, charge carriers hop or tunnel between localized states that are spatially favorable, followed by relaxation. AC conductivity in the temperature range of 90 K–473 K is primarily attributed to the relaxation process induced by quantum mechanical tunneling of charge carriers between localized states. The universal power law behavior of AC conductivity yields an exponent value, s, approximately equal to 0.95 across the entire temperature range (Figure 4(b)), consistent with QMT of charge carriers. The exponent value near unity may be attributed to the non-uniform distribution of localized states in the disordered semiconductor composite system [21, 29]

4. Conclusion:

An investixgation of the electrical transport mechanism in the RGO-ZnSe composite was conducted under varying electric fields. At low frequencies, the real part of the AC conductivity remains constant up to a characteristic frequency, after which it follows a power law behavior. The temperature-independent frequency exponent, s, suggests that phonon-assisted quantum tunneling of charge carriers occurs between defect states in the system. The single semicircle observed in the Cole-Cole plot is indicative of a Debye-like relaxation with a nearly constant relaxation time. Additionally, it was shown that these samples adhere to the time-temperature superposition principle, as evidenced by the universal scaling of conductivity isotherms. These findings not only enhance the fundamental understanding of transport mechanisms in RGO-based composite systems but also motivate further in-depth studies of transport behavior in other disordered materials.

Declaration of Competing Interest: The author declares no known competing financial interests that could have appeared to influence the work reported in this article.

Acknowledgments: The author is thankful to CRF, IIT Kharagpur for SEM and TEM measurements.

References:

[1] V. Singh, D. Joung, L. Zhai, S. Das, S. I. Khondaker, S. Seal, Prog. Mater. Sci., (2011), 56, 1178–1271.
[2] G. Eda, M. Chhowalla, Adv. Mater. (2010), 22, 2392–2415.
[3] D. A. Dikin, S. Stankovich, E. J. Zimney, R. D. Piner, G. H. B. Dommett, G. Evmenenko, S. T. Nguyen, R. S. Ruoff, Nature, (2007), 448, 457–460.
[4] A. Mathkar, D. Tozier, P. Cox, P. Ong, C. Galande, K. Balakrishnan, A. L. M. Reddy, P. M. Ajayan, J. Phys. Chem. Lett. (2012), 3, 986–991.
[5] S. Chakrabarty, K. Chakraborty, A. Laha, T. Pal, S. Ghosh, J. Phys. Chem. C, (2014), 118, 28283–28290.

[6] S. Krishnamurthy, P. V. Kamat, Chem Phys Chem, (2014), 15, 2129–2135.
[7] S. Ghosh, T. Pal, D. Joung, S. I. Khondaker, Appl. Phys. A, (2012), 107, 995-1001.
[8] J. Selvaraj, S. Gupta, S. Dela Cruz, V. Subramanian, Chem Phys Chem, (2014), 15, 2010–2018.
[9] S. C. Rai, K. Wang, Y. Ding, J. K. Marmon, M. Bhatt, Y. Zhang, W. Zhou, Z. L. Wang, ACS Nano, (2015), 9, 6419−6427.
[10] L. Yang, J. Zhu, D. Xiao, RSC Adv. (2012), 2, 8179−8188.
[11] Y. Xi, L. E. Bouanani, Z. Xu, M. A. Quevedo-Lopeza, M. Minary-Jolandan, J. Mater. Chem. C, (2015), 3, 9781−9788.
[12] A. B. Rahaman, A. Sarkar, K. Chakraborty, J. Mukherjee, T. Pal, S. Ghosh, D. Banerjee, J. Phys. Chem. C (2019), 123, 15441−15450.
[13] D. Joung, L. Zhai, S. I. Khondaker, Phys. Rev. B, (2011), 83, 115323.
[14] A. Sarkar, A. B. Rahaman, T. Singha, K. Chakraborty, S. Prodhan, T. Pal, S. Ghosh, P. K. Datta, D. Banerjee, J. Phys. Chem. C, (2020), 124, 7039−7047.
[15] A. Sarkar, A. B. Rahaman, K. Chakraborty, T. Pal, S. Ghosh, D. Banerjee, Appl. Surf. Sci., (2019), 493, 279-286.
[16] K. Chakraborty, P. Das, S. Chakrabarty, T. Pal, S. Ghosh, Chem Phys Chem, (2016), 17, 1518–1523.
[17] W. S. Hummers, R. E. Offema, J. Am. Chem. Soc. (1958), 80, 1339.
[18] S. Sarkar, S. Acharya, A. Chakraborty, and N. Pradhan, J. Phys. Chem. Lett., (2013), 4, 3292–3297.
[19] J. H. Hwang, K. S. Kirkpatrick, T. O. Mason, E. J. Garboczi, Solid State Ionics, (1997), 98, 93–104.
[20] A. Sarkar, A. B. Rahaman, D. Banerjee, J. Phys. D: Appl. Phys. (2018), 51, 095602.
[21] S.R. Elliot, Adv. Phys., (1987), 36, 135–218.
[22] A. K. Jonscher, Nature, (1977), 267, 673.
[23] M. Pollak, T. H. Geballe, Phys. Rev., (1961), 122, 1742.
[24] S. Ghosh, S. Najmaei, S. Kar, R. Vajtai, J. Lou, N. R. Pradhan, L. Balicas, P. M. Ajayan, S. Talapatra, Phys. Rev. B, (2014), 89, 125422.
[25] D. P. Almond, A. R. West, Nature, (1983), 306, 456.
[26] T. Paul, A. Ghosh, J. Appl. Phys., (2018), 123, 045107.
[27] A. Ghosh, A. Pan, Phys. Rev. Lett., (2000), 84, 2188.
[28] J. C. Dyre, Phys. Rev. B, (1993), 47, 91289131.
[29] J. Parui, S.B. Krupanidhi, J. Appl. Phys., (2008),104 (1–11) 024107.